



Lithiophilic LiC₆ Layers on Carbon Hosts Enabling Stable Li Metal Anode in Working Batteries

Peng Shi, Tao Li, Rui Zhang, Xin Shen, Xin-Bing Cheng,* Rui Xu, Jia-Qi Huang,*
Xiao-Ru Chen, He Liu, and Qiang Zhang*

Lithium (Li) metal-based battery is among the most promising candidates for next-generation rechargeable high-energy-density batteries. Carbon materials are strongly considered as the host of Li metal to relieve the powdery/dendritic Li formation and large volume change during repeated cycles. Herein, we describe the formation of a thin lithiophilic LiC₆ layer between carbon fibers (CFs) and metallic Li in Li/CF composite anode obtained through a one-step rolling method. An electron deviation from Li to carbon elevates the negativity of carbon atoms after Li intercalation as LiC₆, which renders stronger binding between carbon framework and Li ions. The Li/CF | Li/CF batteries can operate for more than 90 h with a small polarization voltage of 120 mV at 50% discharge depth. The Li/CF | sulfur pouch cell exhibits a high discharge capacity of 3.25 mAh cm⁻² and a large capacity retention rate of 98% after 100 cycles at 0.1 C. It is demonstrated that the as-obtained Li/CF composite anode with lithiophilic LiC₆ layers can effectively alleviate volume expansion and hinder dendritic and powdery morphology of Li deposits. This work sheds fresh light on the role of interfacial layers between host structure and Li metal in composite anode for long-lifespan working batteries.

High-energy-density batteries are strongly concerned due to the rapid development of portable electronic devices, electric vehicles, and grid-scale energy storage.^[1] Although lithium ion battery (LIB) system based on graphite anode has achieved tremendous success, the relatively low theoretical energy density limits its further applications as the next-generation portable

power sources. Li metal anode has fueled the potential applications of Li metal batteries (LMBs) attributing to its extremely high specific capacity (3860 mAh g⁻¹) and the lowest reduction potential (−3.040 V vs standard hydrogen electrode).^[2] However, the widespread applications of Li metal anode have been severely hindered by multifaceted challenges, such as uncontrolled dendritic/powdered/dead Li and noteworthy volume expansion during repeated Li stripping/plating. These inherent drawbacks significantly reduce the service life of LMBs and even result in catastrophic safety issues.^[3]

Many strategies have been proposed to address these challenges and extend the lifespan of LMBs, including interface modification and introduction of solid-state electrolytes.^[4] However, once high current density and large cycle capacity are applied on a working Li metal anode, the hostless Li electrode experiences a dramatically volumetric change, leading

to failure of solid electrolyte interphase (SEI) attached on a working Li metal anode. In this respect, three-dimensional (3D) hosts with the unique surface chemistry and interconnecting structures are expected to accommodate Li deposition and mitigate volume expansion, thus maintaining the stability of SEI layer and regulating Li plating/stripping behavior effectively.^[5] Therefore, structured metallic Li metal electrode with 3D hosts has been strongly considered as an effective and prospective route to construct stable LMBs with high energy density, long lifespan, and high safety.^[6]

Tremendous progress has been achieved in the rational design of 3D hosts for Li deposition.^[7] The 3D Li metal hosts with lithiophilic sites, such as hollow carbon nanospheres,^[8] MXene,^[9] N-doped graphene,^[10] and edge-rich graphene,^[11] can regulate the Li⁺ nucleation and uniform deposition. Compared with metal-based host (e.g., Ni and Cu), carbon materials are frequently adopted to host Li metal due to their light-weight nature and controllable surface chemistry.^[12] However, these initial Li-free matrices cannot be directly matched with high-energy-density Li-free cathode materials (e.g., sulfur, oxygen, and other Li-free cathodes) at a large capacity.^[13] Li-containing composite anodes are urgently requested for next-generation LMBs.^[14] High-temperature thermal melting method and pre-electrodeposition are usually proposed to fill

P. Shi, Dr. T. Li, R. Zhang, X. Shen, Dr. X.-B. Cheng, X.-R. Chen,
Dr. H. Liu, Prof. Q. Zhang
Beijing Key Laboratory of Green Chemical Reaction
Engineering and Technology
Department of Chemical Engineering
Tsinghua University
Beijing 100084, China
E-mail: cxb12@mails.tsinghua.edu.cn;
zhang-qiang@mails.tsinghua.edu.cn
R. Xu, Prof. J.-Q. Huang
Advanced Research Institute of Multidisciplinary Science
Beijing Institute of Technology
Beijing 100081, China
E-mail: jqhuang@bit.edu.cn



The ORCID identification number(s) for the author(s) of this article can be found under <https://doi.org/10.1002/adma.201807131>.

DOI: 10.1002/adma.201807131

Li metal into pores of 3D host, while these methods are high-risk or very complicated.^[15] Therefore, a facile room-temperature method to fabricate Li-containing composite electrode in large scale is prerequisite for exploration of high-energy-density LMBs. Additionally, the carbon host as the routine anode of LIBs can intercalate Li. The role of the initially formed intercalated Li layer on the subsequent deposition of Li metal should be investigated deeply.

In this contribution, we focus on the interfacial layers in lithium/carbon fiber (Li/CF) composite electrode achieved by subtly rolling ultrathin Li foils into carbon fiber host at room temperature. Uniform and dense LiC_6 interfacial layers are formed on the surface of CF host due to the in situ intercalation reaction between carbon and Li, which benefit the wettability of Li on CF. The electron deviation from Li to carbon elevates the negativity of carbon atoms after Li intercalation as LiC_6 , which renders stronger binding between carbon framework and Li^+ in the electrolyte. Therefore, LiC_6 are demonstrated to be lithiophilic and can guide the Li^+ deposition and improve the stability during the repeated Li plating/stripping cycles (Figure 1). The negative Gibbs free energy of the reaction ($\text{Li} + 6\text{C} \rightarrow \text{LiC}_6$, $-10.59 \text{ kJ mol}^{-1}$) illustrates that the intercalation of Li atoms into carbon is a thermodynamically spontaneous process once metallic Li contacts with CF.^[16] Therefore, the rolling process and generation of lithiophilic LiC_6 both occur at room temperature, which is very convenient to fabricate in large scale and realize the practical application of the composite electrode. The electrochemical performance of Li/CF anode during repeated plating/stripping is comprehensively investigated in symmetrical cells, $\text{Li} | \text{S}$ and $\text{Li} | \text{LiFePO}_4$ (LFP) pouch cells.

The Li/CF composite anode is obtained by facile one-step rolling CF with ultrathin Li foils (Figure S1, Supporting Information). Metallic Li is pressed into the interspace of carbon fibers under rolling pressure (Figure 2a,b and Figure S2, Supporting Information). Abundant macropores and large porosity between fibers promise a high capacity of the composite electrode (Figure 2a). The thickness of the composite anode is

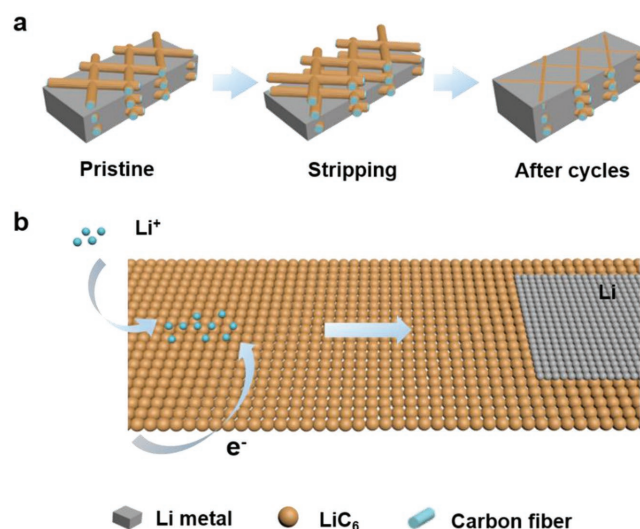


Figure 1. Schematic illustration for a) plating and stripping behavior on Li/CF composite anode and b) the process of adsorption of Li^+ and charge transfer on LiC_6 layers to form uniform Li deposits.

around $125 \mu\text{m}$ (Figure S3, Supporting Information). Notably, the as-obtained composite anode exhibits good flexibility (Figure S4, Supporting Information), rendering the feasible applications in flexible and wearable energy storage devices.^[17]

Once metallic Li is pressed into CF, Li/CF becomes darker compared to pristine CF because the voids in CF are filled by Li (middle panel, Figure 2c). After shelving for 72 h, a thin layer of lithiophilic LiC_6 is formed on the surface of fibers through intrinsic interfacial reactions, accompanied by the change in optical color from black to brownish yellow (right panel, Figure 2c).^[16] No obvious change can be found between pristine and shelved Li/CF in the low-resolution scanning electron microscope (SEM) images (right panel, Figure 2b). Surprisingly, small particles with size of 100–200 nm are uniformly and densely discovered on CF surface after further

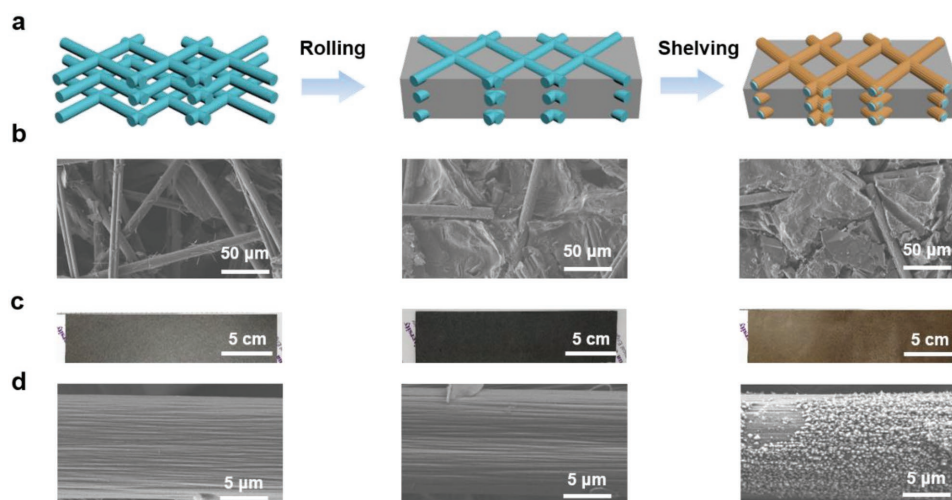


Figure 2. Preparation of Li/CF composite anode and the formation of LiC_6 layers. a) Schematic illustration for pristine CF, initial Li/CF composite anode, and Li/CF composite anode shelving for 72 h with the formation of LiC_6 layers. b) SEM images and c) optical color evolution of pristine CF sheets, Li/CF anode after rolling and shelving for 72 h. d) High-resolution SEM images of single carbon fiber in the pristine, rolled, and shelved CF.

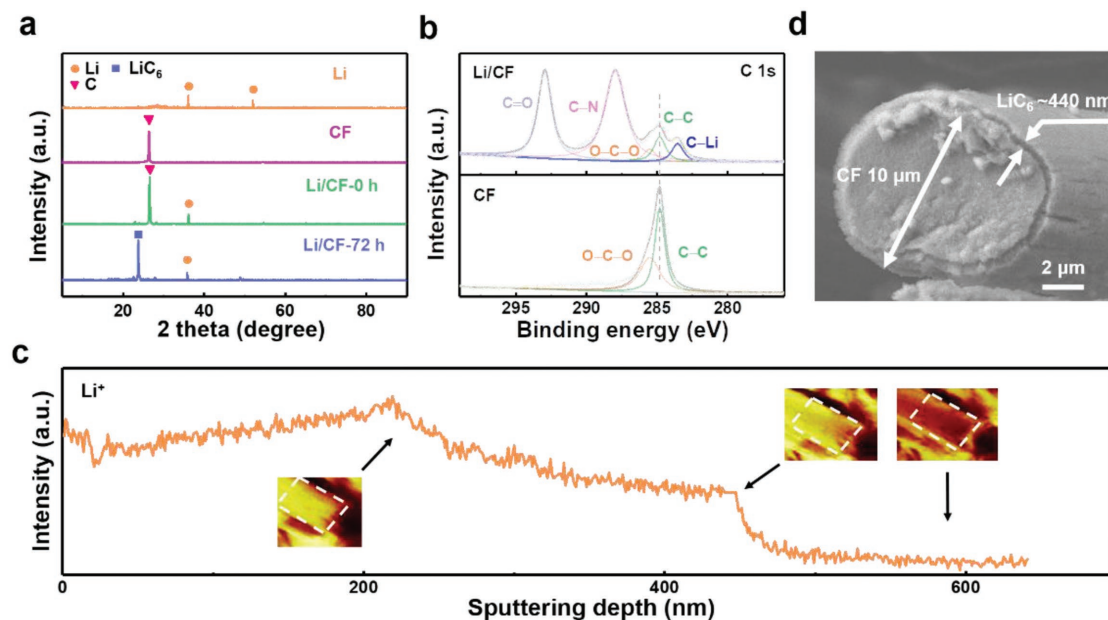


Figure 3. Characterizations of LiC_6 layers. a) XRD patterns of Li, CF, and Li/CF anodes. b) C 1s XPS spectrum of Li/CF anode and pristine CF. c) Li element depth profiles of single CF- LiC_6 fiber and surface image analysis of Li element at different sputtering time by TOF-SIMS. d) Cross-sectional high-resolution SEM images of single CF- LiC_6 fiber.

magnification (right panel, Figure 2d), which can be identified as LiC_6 compounds. The corn-granule-like LiC_6 layers on CF surface construct a 3D interconnected lithiophilic framework in the composite anode (Figure S5, Supporting Information). The excellent ion conductivity and lithiophilicity of LiC_6 layer benefits close contacts between Li metal and CF hosts, which favors dendrite-free plating/stripping behavior during the long cycles.^[16,18]

The chemical components of the interfacial layers are first investigated by the X-ray diffraction (XRD) patterns (Figure 3a). The diffraction peak of pristine CFs is attributed to graphitized carbon. A new peak assigned to LiC_6 appears for Li/CF composite electrode with a shelf time of 72 h.^[19] X-ray photoelectron spectroscopy (XPS) of the composite anode is conducted to further probe the chemistry of LiC_6 layers (Figure 3b). Compared with pristine CF host, three additional peaks in the C 1s spectrum are observed in Li/CF composite anode. The emerging peaks located at 283.5 eV can be assigned to C–Li, which indicates an electron deviation from Li to C. This can also be illustrated by the shift of Li 1s in Li/CF moving to the high field (Figure S6, Supporting Information). The peaks located at 292.2 and 287.9 eV can be assigned to C=O and C–N due to the formation of Li_2CO_3 and Li_3N during sample preparation and characterization, respectively.^[20] The evolution in the radial direction from LiC_6 to CF is investigated by ion sputtering of the time of flight secondary ion mass spectrometry (TOF-SIMS). By analyzing the evolution of Li element count, the thickness of LiC_6 interface layer is about 440 nm (Figure 3c), which is consisted with the results of cross-sectional SEM images (Figure 3d).

The role of lithiophilic LiC_6 layers in regulating nucleation/deposition behavior can be demonstrated by comparing nucleation overpotential and Li plating morphology in pristine CF and CF- LiC_6 electrodes. The CF- LiC_6 electrode is obtained by

removing metallic Li through adding a small amount of anhydrous ethanol into the composite Li/CF electrode. The overpotential of metallic Li plating on Cu foil, CF, and CF- LiC_6 electrodes is recorded (Figure S7, Supporting Information). The profile of CF- LiC_6 electrode exhibits much more smooth voltage dip at the nucleation stage with a nucleation overpotential of only 10 mV. This is much smaller than that of CF electrode (22 mV).

The uniform LiC_6 interfacial layer with strong lithiophilicity on the surface of the CF host promotes a uniform deposition behavior of metallic Li. Due to the difference in the potential of LiC_6 intercalating and metallic Li plating, LiC_6 also forms on CF surface electrochemically. However, the electrochemically formed LiC_6 is much less uniform than the in situ formed LiC_6 on CF surface at room temperature (Figure S8, Supporting Information). This results in islanded deposition in the CF framework compared with the uniform deposition in CF- LiC_6 host (Figure 4a,b). The reduced nucleation overpotential, plating potential, and uniform plating morphology of Li deposits in CF- LiC_6 electrode demonstrate the positive role of lithiophilic LiC_6 on regulating Li nucleation/deposition behavior.

As CF matrix affords abundant macropores to accommodate Li metal, the Li/CF anode delivers a large specific capacity as high as 1841 mAh g^{-1} based on the weight of whole composite anode measured by stripping metallic Li under a current density of 0.5 mA cm^{-2} to 0.6 V (vs Li^+/Li) (Figure S9, Supporting Information).^[21] All Li has been stripped from CF framework, which is confirmed by XRD characterization (Figure S10, Supporting Information). It can be calculated from the different voltage platforms in the stripping process that the capacities contributed by metallic Li and LiC_6 in composite electrode are 8.5 and 1.0 mAh cm^{-2} , respectively. Additionally, the composite electrode can maintain well-defined structure after stripping

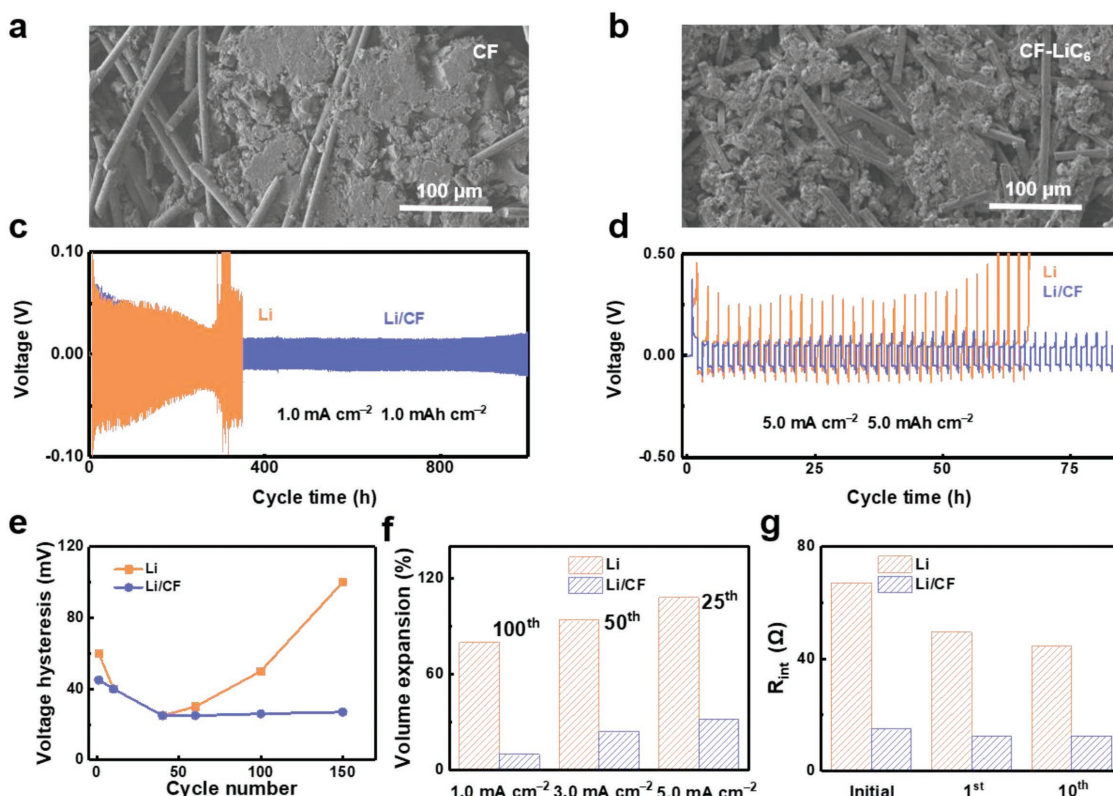


Figure 4. Electrochemical behavior of Li/CF composite anode. The SEM images of a) CF and b) CF-LiC₆ electrode after depositing 3 mAh cm⁻² of Li. Voltage profiles of Li/CF | Li/CF and Li | Li cells with c) a capacity of 1.0 mAh cm⁻² at a current density of 1.0 mA cm⁻² and d) a capacity of 5.0 mAh cm⁻² at a current density of 5.0 mA cm⁻². e) Corresponding voltage hysteresis evolution of panel (c). f) The volume expansion ratio of bare Li and Li/CF anodes after cycling. g) Fitted SEI resistance of bare Li and Li/CF anodes at different cycles.

90% of Li at a current density of 1.0 mA cm⁻² (Figure S11, Supporting Information), verifying the high structural stability of CF framework.

Li/CF | Li/CF symmetrical batteries cycled at different current densities are adopted to investigate the cycling stability of the rolled Li/CF composite electrode with lithiophilic LiC₆ layers. Distinct difference in voltage hysteresis is observed between cells with bare Li and Li/CF electrodes at 1.0 mA cm⁻² with a capacity of 1.0 mAh cm⁻² (Figure 4c,e). The bare Li | Li battery exhibits a gradually increasing hysteresis to 100 mV within 300 h, while the Li/CF | Li/CF cell maintains a much lower and more stable hysteresis of 25 mV after 1000 h. Similar decrease in polarization to 25 mV is observed in these two electrodes at initial 250 h due to the gradual stabilization of SEI layer on Li metal anode. After that, the polarization of bare Li increases sharply relative to that of Li/CF electrode owing to the large volume expansion and thickened “dead” Li layer. The superiority of Li/CF composite electrode can be further confirmed by the outstanding electrochemical performances at high operating current density and cycling capacity (5.0 mA cm⁻², 5.0 mAh cm⁻²). The bare Li foil exhibits a high polarization above 300 mV, while Li/CF electrode presents a polarization of only 120 mV with a stable lifespan over 90 h (Figure 4d). Interestingly, the bare Li | Li battery exhibits an asymmetric polarization curve, which is mainly caused by the large cycling capacity on the bare ultrathin Li electrode. When the cycling capacity is set as 5 mAh cm⁻² (a total electrode capacity is 10 mAh cm⁻² for

the 50 μm ultrathin Li adopted herein), the capacity becomes 15 and 5 mAh cm⁻² for the plating and stripping side after the first discharge process if the side reactions are not considered. The sharp difference in the capacity leads to various cycling behaviors of two electrodes, accounting for the asymmetric polarization curves. Additionally, Li electrodes with the initial plating or stripping processes exhibit different cycling performances after long-term cycles. For the Li/CF electrode, such phenomenon of asymmetric polarization curve is not obvious, demonstrating Li/CF electrode can improve the cycling stability of ultrathin Li electrode and relieve the effect induced by the plating and stripping processes.

The volume expansion after repeated cycles is probed by the cross-sectional images of postern electrodes (Figure 4f and Figure S12, Supporting Information). Bare Li anode exhibits 80% volume expansion after 100 cycles at 1.0 mA cm⁻² and 1.0 mAh cm⁻². In contrast, the volume change is only 10% after 100 cycles for Li/CF composite anode under this condition. Simultaneously, smaller volume expansion at large current densities of 3.0 and 5.0 mA cm⁻² also confirms the long-term stability of Li/CF electrodes. These results prove that the steady lithiophilic LiC₆ layers on the 3D conductive framework and abundant interspaces in CF promise a stable Li plating/stripping behavior at high rates and cycling depth, leading to less “dead” Li and limited volume expansion during the repeated cycles.

Electrochemical impedance spectroscopy (EIS) measurements are applied to obtain the Li⁺ interfacial transport

resistance in Li/CF composite electrode. The bare Li electrode possesses a SEI resistance of around 67 Ω before cycle, which decreases to nearly 49 Ω after the initial cycle (Figure 4g and Figure S13a, Supporting Information). This significant decrease in SEI impedance is caused by the destruction of SEI and exposure of fresh metallic Li due to the large volume shrink of pristine Li foil.^[22] After ten cycles, a new semicircle at low frequency emerges, which is caused by the thickening of “dead” Li layer. On the contrary, the SEI impedance of the Li/CF symmetric battery is only 15 Ω before cycle, one fourth that of bare Li counterpart (Figure S13b, Supporting Information). The much lower SEI impedance in Li/CF composite anode suggests that the strong lithiophilicity of a LiC₆ layer favors higher ionic conductivity. Moreover, the impedance in Li/CF electrode keeps almost constant after ten cycles, demonstrating that limited volume change in Li/CF anode maintains the stability of SEI during the repeated cycles. Considering the lower transportation resistance of Li⁺ in Li/CF composite electrode, a lower hysteresis during repeated cycles and superior stability are expected to be achieved in a working battery with this composite anode. The uniform deposition morphology, reduced polarization/resistance, and limited volume change of Li/CF composite electrode demonstrate the role of lithiophilic LiC₆ layer in achieving superior electrochemical performance.

The LFP and Li | S coin cells are assembled to probe the practical applications of the Li/CF composite anode in full cells. The specific capacity of Li | LFP coin cell rapidly fades to nearly 75 mAh g⁻¹ after 50 cycles (Figure 5a) due to the depletion of limited Li (≈ 10 mAh cm⁻²) and formation of thick layer of “dead” Li with huge volume expansion in Li metal anode (Figure S14a,b, Supporting Information).

In contrast, Li/CF | LFP coin cell exhibits higher and more stable specific capacity than routine Li | LFP cell. The Li/CF | LFP maintains at 120 mAh g⁻¹ for 140 cycles at 1.0 C (1.0 C = 170 mA g⁻¹) with reduced polarization (Figure S15a, Supporting Information), indicating robust ionic and electronic channels in Li/CF composite anode. Compared to the huge volume expansion in bare Li anode, Li/CF anode in full cell experiences much smaller volume change (Figure S14c,d, Supporting Information). The superior cycling performance is attributed to the uniform Li plating/stripping behavior caused by lithiophilic LiC₆ layer in Li/CF composite electrode. Additionally, LiC₆ layers in CF hosts maintain excellent stability during the whole battery lifespan (Figure S16, Supporting Information), illustrating the robustness of Li/CF composite anode.

Li/CF | LFP coin cells also display excellent rate performance compared with bare Li foil (Figure S17, Supporting Information). The discharge capacities of Li/CF | LFP cell reach 151, 146, and 130 mAh g⁻¹ at rates of 0.2 C, 0.5 C, and 1.0 C, respectively, while only 115 mAh g⁻¹ can be achieved at 1.0 C in bare Li | LFP cell.

When the Li/CF composite anodes match S cathodes, the full cells can still exhibit a high capacity and a long lifespan. The initial-specific discharge capacity of Li/CF | S batteries is 751 mAh g⁻¹ at 0.1 C and decreases to 470 mAh g⁻¹ after 400 cycles at a current density of 1 C (1 C = 1675 mA g⁻¹), while the bare Li | S cells only have a capacity of 250 mAh g⁻¹ after 400 cycles (Figure 5b). Similar to Li | LFP batteries, the deteriorated performance of Li | S batteries is induced by huge polarization in the anode side (Figure S15b, Supporting Information). The similar results indicate that the composite anode with LiC₆ layers plays a pivotal role in maintaining the long-term stability in various battery systems.

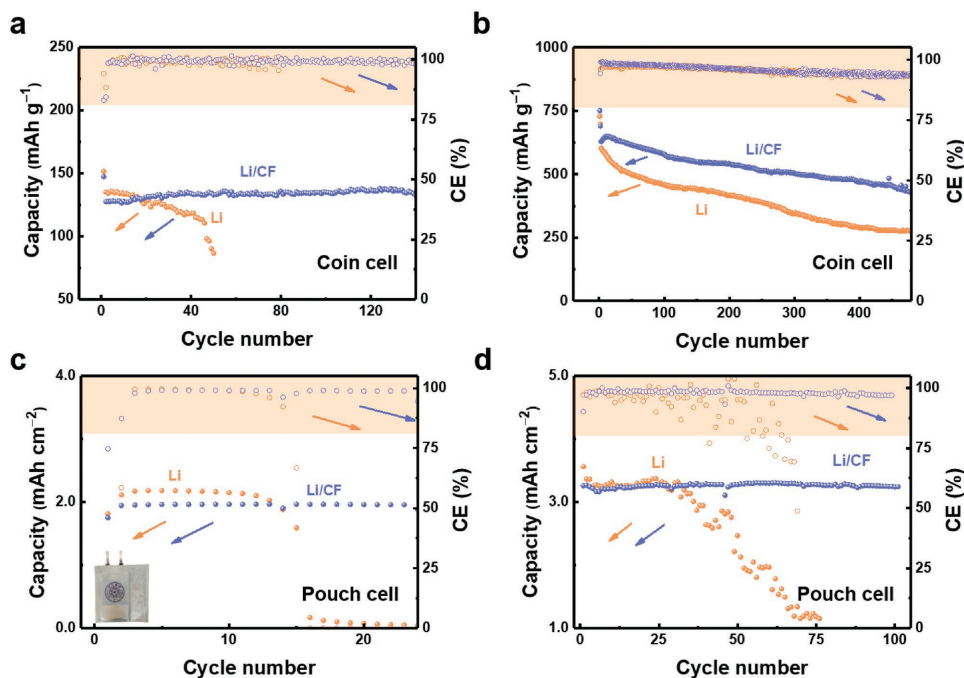


Figure 5. Long-term cycling performance in full cells. Discharge capacity and CE curves at different cycles of a,b) coin and c,d) pouch cells with a,c) LFP and b,d) S cathodes.

Compared to coin cell, pouch cell has more active materials, which is more proper to evaluate the practical applications of Li/CF composite electrode. And the cycling areal and local current density are very large, resulting in a large volume expansion, Li powdering, and short cycling life. The 450 mAh Li | LFP pouch cell with bare Li anode fails after only 13 cycles at 1.0 C due to the extremely uneven local current density and more severe powdering (Figure 5c). While the pouch cell employing Li/CF anode maintains good stability over 20 cycles with a high-capacity retention of 1.8 mAh cm⁻² at 1.0 C. The advantages of the Li/CF composite anode also reflect in Li | S pouch cell. The capacity of the Li/CF | S pouch cell maintains around 3.25 mAh cm⁻² with almost no degradation after 100 cycles and the average Coulombic efficiency (CE) is improved to 98.5% for more than 60 cycles at 0.1 C (Figure 5d and Figure S18, Supporting Information). While bare Li | S pouch cell exhibits huge fluctuations in CE with a rapid decreasing capacity after 20 cycles, indicating the metallic Li has almost completely been consumed with only “dead” Li remained. These results demonstrate that Li/CF composite anode experiences smaller volume change and maintains robust ionic and electronic channels in pouch cells, indicating the potential of the Li/CF composite anode in practical applications.

In conclusion, the Li/CF composite electrode is fabricated by a facile rolling strategy and the role of the in situ formed lithiophilic LiC₆ layers is comprehensively investigated. The formation of LiC₆ interfacial layers realizes a transition from lithiophobic CF to a lithiophilic CF-LiC₆ framework. CF-LiC₆ electrode exhibits a very low nucleation overpotential of only 10 mV. The Li/CF | Li/CF coin cells can even cycle for 90 h at 5.0 mA cm⁻² and 5.0 mAh cm⁻². Full cells matched Li-containing (LFP) and Li-free (S) cathodes both achieve superior electrochemical performance in coin and pouch cells. The Li/CF | LFP coin cells maintains a capacity of 120 mAh g⁻¹ for 140 cycles at 1.0 C with threefold lifespan than that of bare Li | LFP coin cells. Li/CF | S coin cells exhibit a large capacity retention rate of 66% after 400 cycles at 1.0 C. The Li/CF | S pouch cells also present a high discharge capacity of 3.25 mAh cm⁻² and the capacity retention rate over 98% after 100 cycles at 0.1 C. The demonstration of Li/CF electrode with LiC₆ layers in a pouch cell can guide further practical applications of composite Li metal anode in high-energy-density rechargeable batteries. LiC₆ layers reported herein clearly reveal the working model of carbon matrix hosting Li metal. This affords robust energy materials and related energy chemistry for next-generation safe batteries with composite Li metal anodes.

Supporting Information

Supporting Information is available from the Wiley Online Library or from the author.

Acknowledgements

This work was supported by National Key Research and Development Program (2016YFA0202500 and 2015CB932500), National Natural Science Foundation of China (21676160, 21825501, 21805161, and 21808121), and China Postdoctoral Science Foundation (2018M631480 and BX201700125).

Conflict of Interest

The authors declare no conflict of interest.

Keywords

carbon fiber hosts, dendrite-free lithium metal anodes, high-energy-density batteries, lithiophilic LiC₆ layers, nanostructured electrodes

Received: November 4, 2018

Revised: November 24, 2018

Published online:

- [1] a) J. W. Choi, D. Aurbach, *Nat. Rev. Mater.* **2016**, *1*, 16013; b) W. Xu, J. L. Wang, F. Ding, X. L. Chen, E. Nasybutin, Y. H. Zhang, J. G. Zhang, *Energy Environ. Sci.* **2014**, *7*, 513; c) J. B. Goodenough, *Energy Storage Mater.* **2015**, *1*, 158.
- [2] a) X. B. Cheng, R. Zhang, C. Z. Zhao, Q. Zhang, *Chem. Rev.* **2017**, *117*, 10403; b) P. G. Bruce, S. A. Freunberger, L. J. Hardwick, J. M. Tarascon, *Nat. Mater.* **2012**, *11*, 19; c) X. Shen, H. Liu, X.-B. Cheng, C. Yan, J.-Q. Huang, *Energy Storage Mater.* **2018**, *12*, 161; d) L. Wang, Z. Zhou, X. Yan, F. Hou, L. Wen, W. Luo, J. Liang, S. X. Dou, *Energy Storage Mater.* **2018**, *14*, 22.
- [3] D. C. Lin, Y. Y. Liu, Y. Cui, *Nat. Nanotechnol.* **2017**, *12*, 194.
- [4] a) Y. Liu, G. Zhou, K. Liu, Y. Cui, *Acc. Chem. Res.* **2017**, *50*, 2895; b) C. Luo, X. Ji, J. Chen, K. J. Gaskell, X. He, Y. Liang, J. Jiang, C. Wang, *Angew. Chem., Int. Ed.* **2018**, *57*, 8567; c) X. Q. Zhang, X. B. Cheng, X. Chen, C. Yan, Q. Zhang, *Adv. Funct. Mater.* **2017**, *27*, 1605989; d) Y. Y. Lu, S. K. Das, S. S. Moganty, L. A. Archer, *Adv. Mater.* **2012**, *24*, 4430; e) C. Z. Zhao, X. Q. Zhang, X. B. Cheng, R. Zhang, R. Xu, P. Y. Chen, H. J. Peng, J. Q. Huang, Q. Zhang, *Proc. Natl. Acad. Sci. USA* **2017**, *114*, 11069; f) Q. Li, H. Y. Pan, W. J. Li, Y. Wang, J. Y. Wang, J. Y. Zheng, X. Q. Yu, H. Li, L. Q. Chen, *ACS Energy Lett.* **2018**, *3*, 2259; g) X. L. Fan, L. Chen, O. Borodin, X. Ji, J. Chen, S. Hou, T. Deng, J. Zheng, C. Y. Yang, S. C. Liou, K. Amine, K. Xu, C. S. Wang, *Nat. Nanotechnol.* **2018**, *13*, 715; h) X. Zhang, X. Chen, X. Cheng, B. Li, X. Shen, C. Yan, J. Huang, Q. Zhang, *Angew. Chem., Int. Ed.* **2018**, *57*, 5301.
- [5] a) Z. W. Sun, S. Jin, H. C. Jin, Z. Z. Du, Y. Zhu, A. Y. Cao, H. X. Ji, L. J. Wan, *Adv. Mater.* **2018**, *30*, 1800884; b) T. Foroozan, F. A. Soto, V. Yurkiv, S. Sharifi-Asl, R. Deivanayagam, Z. N. Huang, R. Rojaee, F. Mashayek, P. B. Balbuena, R. Shahbazian-Yassar, *Adv. Funct. Mater.* **2018**, *28*, 1705917.
- [6] R. Zhang, X. Chen, X. Shen, X. Q. Zhang, X. R. Chen, X. B. Cheng, C. Yan, C. Z. Zhao, Q. Zhang, *Joule* **2018**, *2*, 764.
- [7] a) C. Zhang, Z. J. Huang, W. Lv, Q. B. Yun, F. Y. Kang, Q. H. Yang, *Carbon* **2017**, *123*, 744; b) R. Zhang, N. W. Li, X. B. Cheng, Y. X. Yin, Q. Zhang, Y. G. Guo, *Adv. Sci.* **2017**, *4*, 1600445; c) Y. Zhang, W. Luo, C. Wang, Y. Li, C. Chen, J. Song, J. Dai, E. M. Hitz, S. M. Xu, C. P. Yang, Y. B. Wang, L. B. Hu, *Proc. Natl. Acad. Sci. USA* **2017**, *114*, 3584; d) L. Liu, Y. X. Yin, J. Y. Li, N. W. Li, X. X. Zeng, H. Ye, Y. G. Guo, L. J. Wan, *Joule* **2017**, *1*, 563.
- [8] G. Zheng, S. W. Lee, Z. Liang, H. W. Lee, K. Yan, H. Yao, H. Wang, W. Li, S. Chu, Y. Cui, *Nat. Nanotechnol.* **2014**, *9*, 618.
- [9] B. Li, D. Zhang, Y. Liu, Y. X. Yu, S. M. Li, S. B. Yang, *Nano Energy* **2017**, *39*, 654.
- [10] R. Zhang, X. R. Chen, X. Chen, X. B. Cheng, X. Q. Zhang, C. Yan, Q. Zhang, *Angew. Chem., Int. Ed.* **2017**, *56*, 7764.
- [11] Q. Song, H. B. Yan, K. D. Liu, K. Y. Xie, W. Li, W. H. Gai, G. H. Chen, H. J. Li, C. Shen, Q. G. Fu, S. Y. Zhang, L. L. Zhang, B. Q. Wei, *Adv. Energy Mater.* **2018**, *8*, 1800564.

- [12] S. Liu, A. X. Wang, Q. Q. Li, J. S. Wu, K. V. Chiou, J. X. Huang, J. Y. Luo, *Joule* **2018**, *2*, 184.
- [13] Z. Liang, G. Y. Zheng, C. Liu, N. Liu, W. Y. Li, K. Yan, H. B. Yao, P. C. Hsu, S. Chu, Y. Cui, *Nano Lett.* **2015**, *15*, 2910.
- [14] Y. M. Sun, N. A. Liu, Y. Cui, *Nat. Energy* **2016**, *1*, 16071.
- [15] W. Deng, W. Zhu, X. Zhou, X. Peng, Z. Liu, *ACS Appl. Mater. Interfaces* **2018**, *10*, 20387.
- [16] Y. J. Shao, H. C. Wang, Z. L. Gong, D. W. Wang, B. Z. Zheng, J. P. Zhu, Y. X. Lu, Y. S. Hu, X. X. Guo, H. Li, X. J. Huang, Y. Yang, C. W. Nan, L. Q. Chen, *ACS Energy Lett.* **2018**, *3*, 1212.
- [17] K. Liu, B. Kong, W. Liu, Y. M. Sun, M. S. Song, J. Chen, Y. Y. Liu, D. C. Lin, A. Pei, Y. Cui, *Joule* **2018**, *2*, 1857.
- [18] H. Ye, S. Xin, Y. X. Yin, J. Y. Li, Y. G. Guo, L. J. Wan, *J. Am. Chem. Soc.* **2017**, *139*, 5916.
- [19] Y. Sun, G. Zheng, Z. W. Seh, N. Liu, S. Wang, J. Sun, H. R. Lee, Y. Cui, *Chem* **2016**, *1*, 287.
- [20] Y. J. Zhang, X. H. Xia, D. H. Wang, X. L. Wang, C. D. Gu, J. P. Tu, *RSC Adv.* **2016**, *6*, 11657.
- [21] S. F. Liu, X. H. Xia, S. J. Deng, L. Y. Zhang, Y. Q. Li, J. B. Wu, X. L. Wang, J. P. Tu, *Energy Storage Mater.* **2018**, *15*, 31.
- [22] D. P. Lv, Y. Y. Shao, T. Lozano, W. D. Bennett, G. L. Graff, B. Polzin, J. G. Zhang, M. H. Engelhard, N. T. Saenz, W. A. Henderson, P. Bhattacharya, J. Liu, J. Xiao, *Adv. Energy Mater.* **2015**, *5*, 1402290.